PROC. OF JSCE,
No. 307, March 1981

OSCILLATION SAND RIPPLES IN VISCOUS FLUIDS

By Arata KANEKO

1. INTRODUCTION

The sand ripples induced under oscillatory flow and water waves have been a subject of practical interest in connection with the sand transport in a nearshore region. On the basis of experiments, Bagnold[1] classified oscillation sand ripples into two types of 'rolling-grain ripples' and 'vortex ripples', and discussed two characteristic length-scales of the ripples, the wavelength L and the waveheight H. Since then various properties of oscillation sand ripples have been clarified by using mainly experimental procedures and dimensional analyses[2)~12)]. However, no basic mechanism determining the length-scales of ripples has been elucidated[13)]. The oscillatory viscous flow over ripples is characterized by two representative length-scales, the stroke (twice the amplitude) of fluid oscillation d_0 and the thickness of the Stokes layer δ. In contrast to the effect of d_0 on L, the effect of δ has been long overlooked. The clarification of δ dependence seems to be necessary for a better understanding of the basic mechanism. Chan et al.[14] observed oscillation sand ripples under various fluids and bed materials, but the flow induced over the ripples and the δ dependence of L and H were not examined. Uda & Hino[15] and Sleath[16] analysed an oscillatory viscous flow of small amplitudes over a rigid wavy wall using a procedure similar to that of Lyne[17]. Although L of ripples with a maximum growth rate was discussed in the different processes of analysis, any direct comparisons with observations were not attempted. In preceding papers of Kaneko & Honji[18),19)], it was reported that a mono-layer of particles scattered sparsely on a smooth plane floor grows into the so called 'particle waves' under oscillatory flow, and that in a highly viscous fluid the oscillation sand ripples are made up inducing steady streamings similar to those computed by extending Lyne's theory. Kaneko & Matsunaga[20] also estimated numerically the wavelength of such ripples which induce steady streamings.

The main purpose of this study is to clarify the effect of δ on ripple formation by varying the fluid viscosity in a wide range of its value. The detailed computations on oscillatory flow over ripples and L of ripples are made using the previous analytical procedure[20], and the computed results are compared with the observed ones in viscous fluids. The methods of experiments and numerical analysis are described in §2. and §3., respectively. In §4.(1), the computed streaming patterns are presented and compared with those observed above real ripples. A grouping and length-scales of ripples are discussed in §§ 4.(2) and 4.(3), respectively.

2. EXPERIMENTS

The experiments were made using a closed-type tunnel and a U-tube, in which a fluid was oscillated by a piston. Details of the apparatus are presented in the preceding papers[18),19)]. The cross sections of the test section of the tunnel and the U-tube were 15×15 cm and 12×12 cm, respectively, and the stroke of fluid oscillation in the both apparatus was about 14 cm. The maximum frequencies for the tunnel and the tube were 1.7 Hz and 2.5 Hz, respectively. Tap water and glycerine-water solutions were used as working fluids. The oscillation sand ripples and the particle waves under glycerine-water solutions were observed mainly by using the U-tube. The kinematic viscosity of the solutions was varied up to 2.08 cm^2/s. Spherical glass beads of specific gravity 2.43 and median diameter 0.006–0.5 cm were used as bed materials.

3. NUMERICAL ANALYSIS

The oscillatory viscous flow over a rigid wavy wall is analysed by using a perturbation method together with a finite difference method. Let us consider the vorticity equation for two-dimensional oscillatory flow over an infinite wavy wall. We shall make use of rectangular cartesian coordinates (x, y), as sketched in **Fig. 1**. Let t denote time and Ψ a stream function. We intro-

* Member of JSCE, M. Eng., Research Associate, Research Institute for Applied Mechanics, Kyushu University.

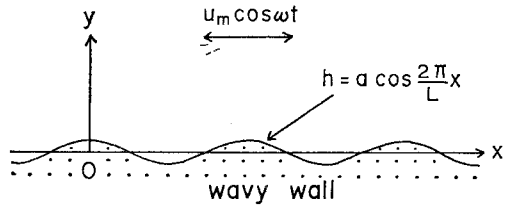

Fig. 1 Coordinate System.

duce the following nondimensional quantities

$$\left.\begin{aligned} &\hat{\phi}=\Psi/u_m\delta \qquad \xi=x/L \qquad \eta=y/\delta \\ &\tau=\omega t \quad \epsilon=d_0/L \quad \beta=L/\delta \quad \eta_0=h/\delta \end{aligned}\right\} \cdots\cdots(1)$$

in which $\delta(=\sqrt{2\nu/\omega})$ is the thickness of the Stokes layer, L the wall wavelength, and ν the kinematic viscosity of a fluid. The quantities u_m, ω and d_0 are the maximum flow velocity, the angular frequency, and the oscillation stroke of a fluid as $\eta\to\infty$, respectively. The basic equation in a nondimensional form is

$$2\frac{\partial}{\partial\tau}(\nabla^2\hat{\phi})-\epsilon\frac{\partial(\hat{\phi},\nabla^2\hat{\phi})}{\partial(\xi,\eta)}=\nabla^2(\nabla^2\hat{\phi}) \cdots\cdots(2)$$

in which symbol $\partial(\hat{\phi},\nabla^2\hat{\phi})/\partial(\xi,\eta)$ denotes Jacobian and $\nabla^2=\partial^2/\partial\eta^2+1/\beta^2\cdot\partial^2/\partial\xi^2$. A profile of the wall is given by

$$\eta_0=\alpha\cos 2\pi\xi \cdots\cdots(3)$$

in which $\alpha=a/\delta$ and a is the amplitude of the wall. It is seen from Eqs. (2) and (3) that flow structures over the wall depend only on three nondimensional parameters ϵ, α and β. The boundary conditions for Eq. (2) may be taken as

$$\left.\begin{aligned} &\hat{\phi}=\partial\hat{\phi}/\partial\eta=0 \qquad \text{on } \eta=\eta_0 \\ &\partial\hat{\phi}/\partial\eta\to\cos\tau \quad \partial\hat{\phi}/\partial\xi\to 0 \quad \text{as } \eta\to\infty \end{aligned}\right\} \cdots\cdots(4)$$

According to Kaneko & Honji[19], the steady streamings induced above the wall under the condition of $\epsilon\ll 1$ show up double structures in $\beta>26$ and its value does not depend on a parameter α. Attention is focused on the case of $\alpha\ll 1$ to clarify the effect of increasing ϵ on flow structures. We expand the solution of Eq. (2) ($\hat{\phi}$) in a form

$$\hat{\phi}=\Psi_0+\alpha\psi \cdots\cdots(5)$$

Substituting Eq. (5) into (2), we obtain a linearized equation

$$2\frac{\partial}{\partial\tau}(\nabla^2\psi)+\epsilon\left[F(\eta,\tau)\frac{\partial}{\partial\xi}(\nabla^2\psi)-G(\eta,\tau)\frac{\partial\psi}{\partial\xi}\right]=\nabla^2(\nabla^2\psi) \cdots\cdots(6)$$

The functions F and G are given by the solution Ψ_0 for a primary flow as follows

$$\left.\begin{aligned} F(\eta,\tau)&=\partial\Psi_0/\partial\eta \\ &=R[(1-\exp\{-(1+i)\eta\})\exp(i\tau)] \\ G(\eta,\tau)&=\partial^3\Psi_0/\partial\eta^3 \\ &=-R[2i\exp\{-(1+i)\eta\}\exp(i\tau)] \end{aligned}\right\} \cdots\cdots(7)$$

in which R denotes 'real part of'. We further expand ψ in a form

$$\psi=\sum_{m=0}^{\infty}\epsilon^m\psi_m \cdots\cdots(8)$$

Substituting Eq. (8) into (6) and equating like powers of ϵ, we obtain the equations

$$\left.\begin{aligned} &2\frac{\partial}{\partial\tau}(\nabla^2\psi_0)=\nabla^2(\nabla^2\psi_0) \qquad \text{for } m=0 \\ &2\frac{\partial}{\partial\tau}(\nabla^2\psi_m)+F\frac{\partial}{\partial\xi}(\nabla^2\psi_{m-1}) \\ &\quad -G\frac{\partial\psi_{m-1}}{\partial\xi}=\nabla^2(\nabla^2\psi_m) \qquad \text{for } m\geqq 1 \end{aligned}\right\} \cdots\cdots(9)$$

We introduce here the vorticity Ω_m as

$$\nabla^2\psi_m=-\Omega_m \qquad \text{for } m\geqq 0 \cdots\cdots(10)$$

Substituting Eq. (10) into (9), we obtain

$$2\frac{\partial\Omega_m}{\partial\tau}+F\frac{\partial\Omega_{m-1}}{\partial\xi}+G\frac{\partial\psi_{m-1}}{\partial\xi}=\nabla^2\Omega_m \qquad \text{for } m\geqq 1 \cdots\cdots(11)$$

in which the solutions ψ_0 and Ω_0 are determined from the equations for $m=0$ in Eqs. (9) and (10) as follows

$$\left.\begin{aligned} \psi_0&=R\left[\frac{1+i}{\sigma-2\pi/\beta}\{\exp(-\sigma\eta)\right. \\ &\quad \left.-\exp(-2\pi\eta/\beta)\}\exp(i\tau)\cos 2\pi\xi\right] \\ \Omega_0&=-R[(1+i)(\sigma+2\pi/\beta) \\ &\quad \cdot\exp(-\sigma\eta)\exp(i\tau)\cos 2\pi\xi] \end{aligned}\right\} \cdots\cdots(12)$$

with $\sigma=\{(2\pi/\beta)^2+2i\}^{1/2}$. The initial conditions are

$$\psi_m(\xi,\eta,0)=\Omega_m(\xi,\eta,0)=0 \cdots\cdots(13)$$

The boundary conditions for η are

$$\left.\begin{aligned} &\psi_m=0 \quad \Omega_m=-\partial^2\psi_m/\partial\eta^2 \quad \text{at } \eta=0 \\ &\psi_m\to 0 \quad \Omega_m\to 0 \quad \text{as } \eta\to\infty \end{aligned}\right\} \cdots\cdots(14)$$

The conditions

$$\left.\begin{aligned} &\psi_m(\xi,\eta,\tau)=\psi_m(\xi+1,\eta,\tau) \\ &\Omega_m(\xi,\eta,\tau)=\Omega_m(\xi+1,\eta,\tau) \end{aligned}\right\} \cdots\cdots(15)$$

are imposed since the flow is periodic with respect to ξ. We define the stream function for steady streamings (ψ_s) as

$$\left.\begin{aligned} &\psi_s^{(p)}=\frac{1}{2\pi}\int_{2p\pi}^{2(p+1)\pi}\alpha\sum_{m=1}^{\infty}\epsilon^m\psi_m(\xi,\eta,\tau)d\tau \\ &\psi_s^{(p)}\longrightarrow\psi_s \quad \text{as } p\to\infty \end{aligned}\right\} \cdots\cdots(16)$$

in which p is an integer. The wall shear stress (τ_s) due to ψ_s is given by a relation

$$\hat{\tau}_s=\frac{\tau_s}{\rho u_m\nu/\delta}=\frac{\partial^2\psi_s}{\partial\eta^2} \qquad \text{at } \eta=0 \cdots\cdots(17)$$

in which $\hat{\tau}_s$ is a nondimensional wall shear stress. Integrating τ_s over half a wavelength and putting its value into τ_s^*, we obtain a relation

$$\hat{\tau}_s^*=\frac{\tau^{2*}}{\rho u_m \nu}=\beta\int_{1/2}^{1}\frac{\partial^2\psi_s}{\partial\eta^2}d\xi \quad \text{at} \quad \eta=0 \cdots(18)$$

By using the advancing difference schemes for the time differential and the central difference schemes for the space differential, Eq. (11) is approximated by the equation

$$\begin{aligned}\Omega^{(n+1)}_{m,i,j}=&\left[1-\left\{\frac{1}{(\Delta\eta)^2}+\frac{1}{(\beta\Delta\xi)^2}\right\}\Delta\tau\right]\Omega^{(n)}_{m,i,j}\\&+\frac{\Delta\tau}{2(\Delta\eta)^2}(\Omega^{(n)}_{m,i,j+1}+\Omega^{(n)}_{m,i,j-1})\\&+\frac{\Delta\tau}{2(\beta\Delta\xi)^2}(\Omega^{(n)}_{m,i+1,j}+\Omega^{(n)}_{m,i-1,j})\\&-\frac{F^{(n)}_{i,j}\Delta\tau}{4\Delta\xi}(\Omega^{(n)}_{m-1,i+1,j}-\Omega^{(n)}_{m-1,i-1,j})\\&-\frac{G^{(n)}_{i,j}\Delta\tau}{4\Delta\xi}(\psi^{(n)}_{m-1,i+1,j}-\psi^{(n)}_{m-1,i-1,j})\end{aligned} \cdots\cdots(19)$$

in which $(\xi, \eta, \tau)=(i\Delta\xi, j\Delta\eta, n\Delta\tau)$. Lattice points $(i, 1)$ correspond to the points at $\eta=0$, and $(1, j)$ and (M, j) to the points above two neighbouring crests of the wall. The difference schemes can be shown to be stable under the following condition

$$\left\{\frac{1}{(\Delta\eta)^2}+\frac{1}{(\beta\Delta\xi)^2}\right\}\Delta\tau\leqq 1 \cdots\cdots(20)$$

By using the succesive over relaxation (SOR) method[21], Eq. (10) is approximated as

$$\begin{aligned}\psi^{(n,k+1)}_{m,i,j}=&\psi^{(n,k)}_{m,i,j}+\frac{w}{2[1+(\Delta\eta/\beta\Delta\xi)^2]}[\psi^{(n,k)}_{m,i,j+1}\\&+\psi^{(n,k+1)}_{m,i,j-1}+(\Delta\eta/\beta\Delta\xi)^2(\psi^{(n,k)}_{m,i+1,j}\\&+\psi^{(n,k+1)}_{m,i-1,j})-2\{1+(\Delta\eta/\beta\Delta\xi)^2\}\\&\cdot\psi^{(n,k)}_{m,i,j}+(\Delta\eta)^2\Omega^{(n)}_{m,i,j}]\end{aligned} \cdots\cdots(21)$$

in which a relaxation parameter w is taken as 1.8 in the computation. The superscript k denotes the number of iterations which are repeated until

$$\frac{\mathrm{Max}\{\psi^{(n,k+1)}_{m,i,j}-\psi^{(n,k)}_{m,i,j}\}}{\mathrm{Max}\{\psi^{(n,k)}_{m,i,j}\}}<10^{-4} \cdots\cdots(22)$$

is satisfied. The vorticity $\Omega^{(n)}_{m,i,1}$ and the wall shear stress $\hat{\tau}_{s,i,1}$ are approximated by the relations

$$\begin{aligned}\Omega^{(n)}_{m,i,1}&=-\frac{8\psi^{(n)}_{m,i,2}-\psi^{(n)}_{m,i,3}}{2(\Delta\eta)^2}\\ \hat{\tau}_{s,i,1}&=\frac{8\psi_{s,i,2}-\psi_{s,i,3}}{2(\Delta\eta)^2}\end{aligned} \cdots\cdots(23)$$

The computation was made in the region of $\eta<2\beta$, i.e. $y<2L$ beyond which the flow disturbances due to the wavy wall were not diffused. $\Delta\eta$ should be less than 1 for sufficient computational accuracy.

4. RESULTS AND DISCUSSION

(1) Flows over Ripples

The classification of oscillation sand ripples by Bagnold[1] was based on whether flow separation from ripple crests exists or not. The rolling-grain ripples have been considered as ripples which do not accompany with flow separation because of small waveheights. No detailed observations of the flow over the ripples have been made. It was reported based on observations by Honji et al.[22] that steady streamings have a role similar to separation vortices in ripple formation. The computed patterns of the streamings are discussed here. The flow patterns are drawn over one wavelength ranging from crest to crest.

Fig. 2 shows the time variation of streaming patterns computed based on Eqs. (19) and (21) under the conditions $\epsilon=0.6$ and $\beta=15$. The terms up to ϵ^5 are considered in the computation. The number of lattice points used in this computation is 11×37. It is seen from **Figs. 2**(c) and (d) that the streaming patterns become stationary at 8 cycles of oscillation. **Fig. 3** shows the flow pattern of steady streamings observed under the conditions $\epsilon=0.6$, $\alpha=0.6$ and $\beta=18$, ϵ and β being roughly equal to those of **Fig. 2.** Since the observed pattern is similar to the computed one, the flow over the real ripples is almost the same as that over the rigid wavy wall. The double structure of steady streamings in **Fig. 2** (d) appears at β smaller than its critical value of 26 determined by Kaneko & Honji[19] when $\epsilon\ll1$, and the appearance is due to the effect of increasing ϵ. Similarly to separation vortices, a pair of lower recirculations rotates in such a way that the flow along the slopes of ripples is from trough to crest and dominates the development of ripples.

Fig. 4 shows a series of streaming patterns computed at $\beta=15$, 18 and 21, and at $\epsilon=0.3$. All the streamings show the patterns obtained at 8 cycles of oscillation. The terms up to ϵ^3 are considered in all the computations. The number of lattice points is 11×51 in all cases. A comparison between **Figs 2** and **4** shows that the double structure appears at a smaller β as ϵ increases.

Total masses of sand transport relating to the development of ripples may depend mainly on $\hat{\tau}_s^*$. The numerical values of $\hat{\tau}_s^*$ are shown in **Figs. 5**(a) and (b). **Fig. 5**(a) shows the results computed at $\alpha=0.1$, 0.3 and 0.5, and at $\epsilon=0.1$ based on the perturbation theory of Kaneko & Honji[19]. All the curves drawn for each value of α show that the value of $\hat{\tau}_s^*$ increases with β and reaches the maximum values immediately after the double structure of steady streamings appears. The value of α does not affect the critical value of β for the appearance of the double structure and $(\hat{\tau}_s^*)_{\max}$. The result of the present analysis at

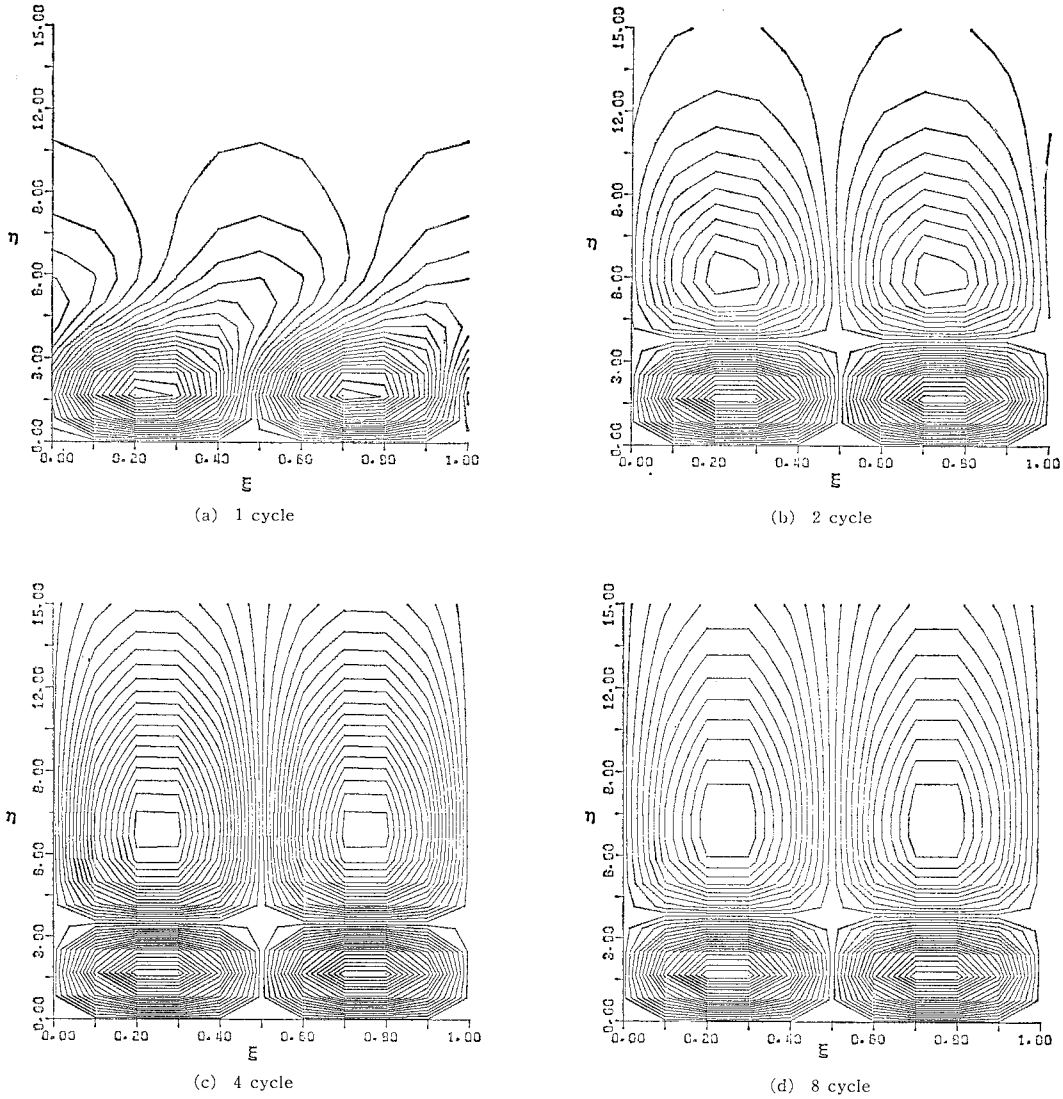

(a) 1 cycle (b) 2 cycle

(c) 4 cycle (d) 8 cycle

Fig. 2 Time Variations of Streaming Patterns at $\epsilon=0.6$ and $\beta=15$.

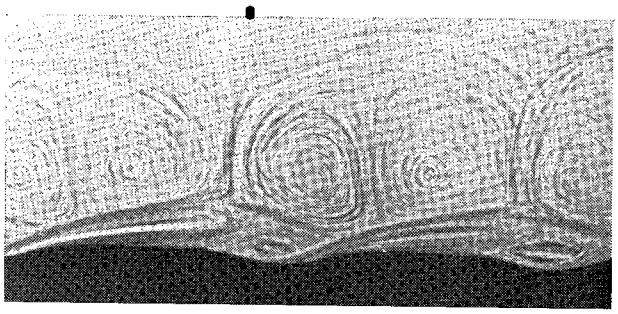

Fig. 3 Streaming Pattern Photographed at $\epsilon=0.6$, $\alpha=0.6$ and $\beta=18$.

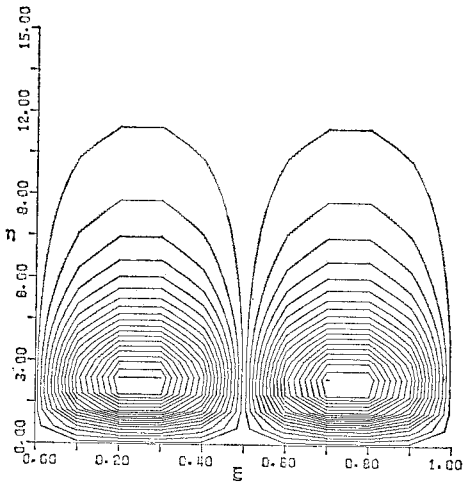

(a) $\beta=15$

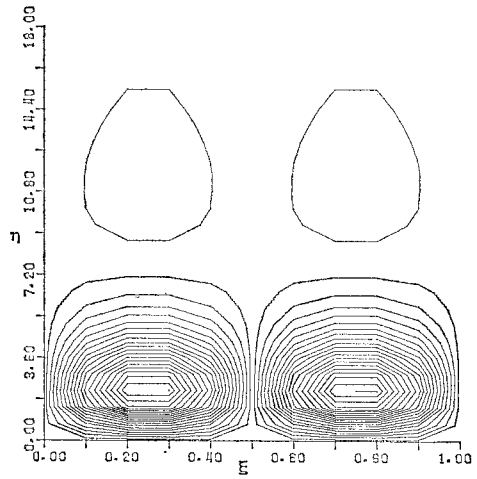

(b) $\beta=18$

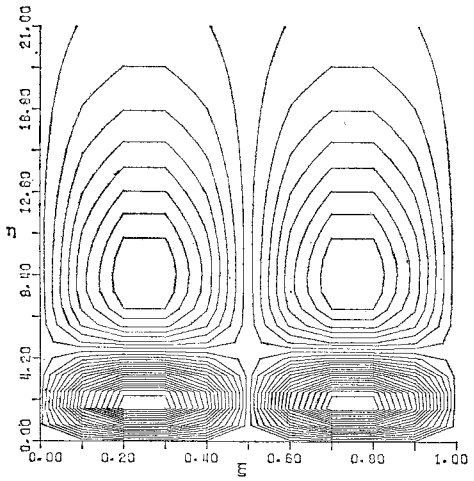

(c) $\beta=21$

Fig. 4 Variations of Streaming Patterns with β ($\epsilon=0.3$).

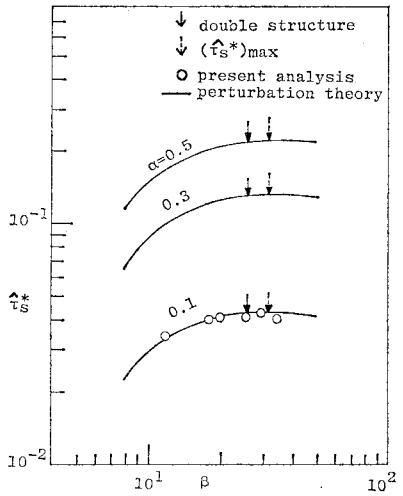

(a) Analyses for small oscillation amplitudes ($\varepsilon=0.1$).

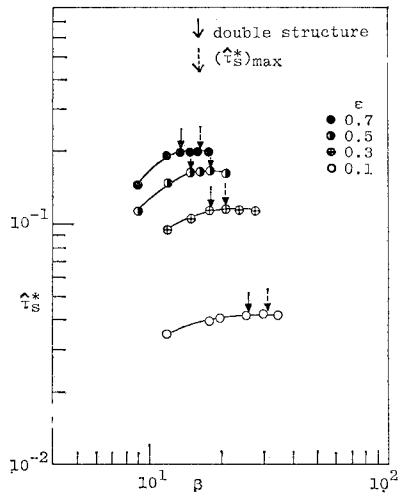

(b) Present analysis for small waveheights ($\alpha=0.1$).

Fig. 5 Calculation of Wall Shear Stresses.

$\epsilon=0.1$ and $\alpha=0.1$ is also plotted in **Fig. 5**(a). Since the plotted data agree well with the curve for $\alpha=0.1$, it is seen that the computational accuracy is sufficient. The result of the present analysis for larger ϵ is plotted in **Fig. 5**(b). The solid lines are also drawn through the plotted data. The double structure and $(\hat{\tau}_s^*)_{max}$ appear at a smaller β as ϵ increases. The critical condition for the appearance of $(\hat{\tau}_s^*)_{max}$ is well approximated by a simple relation

$$\frac{L}{d_0}=\frac{50.6}{(d_0/\delta)^{1.48}} \quad \cdots\cdots(24)$$

in which $L/d_0=1/\epsilon$ and $d_0/\delta=\epsilon\beta$. Equation (24) is later compared with the wavelength of real ripples in a highly viscous fluid.

(2) Grouping of Ripples

The wave patterns in a mono-layer of particles scattered sparsely on a smooth plane floor are discussed first as a simple system of rolling-grain ripples. **Fig. 6** (a) shows a typical pattern of particle waves, and **Fig. 6** (b) a wave pattern formed when a fluid oscillates slowly at large amplitudes. The wave pattern of **Fig. 6** (b) is composed of clusters of the particles, which may be called 'particle spots'. Since the particles in these waves do not pile-up in contrast to those in rolling-grain ripples, the waveheight is equal to the particle diameter.

Consider the motion of particles on a smooth plane floor. The initiation of the particle motion in an oscillatory flow may be correlated with the following independent variables

$$u_m, \omega, \nu, g, D, \rho, \quad \text{and} \quad \rho_s \cdots\cdots\cdots\cdots (25)$$

in which ρ_s is the density of particles and ρ that of a fluid. D is the particle diameter and g the acceleration due to gravity. Based on the dimensional analysis, we obtain a relation among four nondimensional variables

$$\frac{u_m}{\sqrt{(\rho_s/\rho-1)gD}}=F\left(\frac{D}{\delta},\ \frac{u_mD}{\nu},\ \frac{\rho_s}{\rho}\right) \cdots (26)$$

in which F stands for a function. Considering that ρ_s/ρ is nearly constant in the present experiments, we retain it only in the left-hand side of Eq. (26) to obtain

$$\frac{u_m}{\sqrt{(\rho_s/\rho-1)gD}}=F'\left(\frac{D}{\delta},\ \frac{u_mD}{\nu}\right) \cdots\cdots (27)$$

in which $u_m/\sqrt{(\rho_s/\rho-1)gD}$ is the Shields relative stress criterion modified for oscillatory flow, D/δ the relative roughness of particles and u_mD/ν the particle Reynolds number. Symbol F' stands for a function.

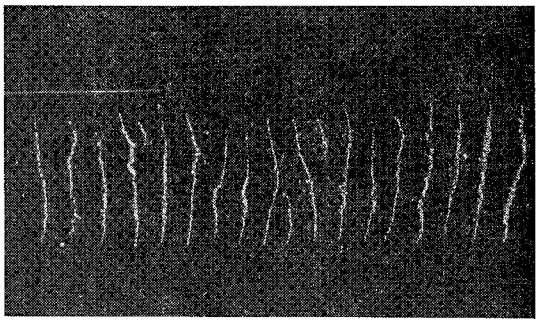

(a) Particle wave

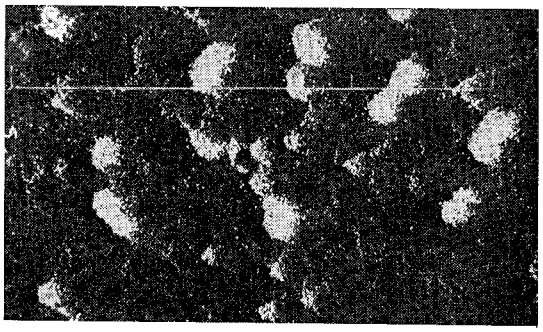

(b) Particle spot

Fig. 6 Two Typical Patterns of Particles.

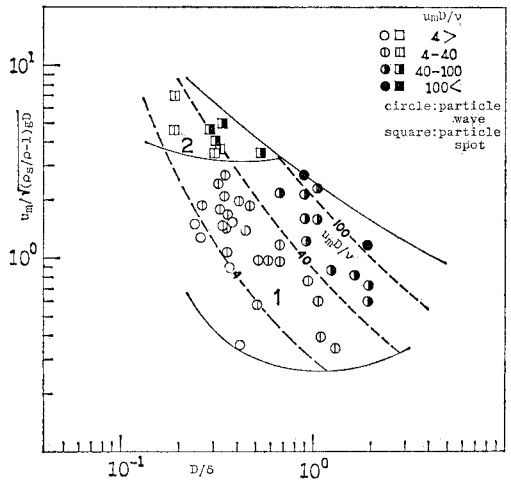

Fig. 7 Formation Regions of Particle Patterns.

On the basis of Eq. (27) and the results of present experiments, the values of $u_m/\sqrt{(\rho_s/\rho-1)gD}$ at which the wave patterns formed are plotted against D/δ in **Fig. 7**. The distribution of the plotted data makes it possible to draw the formation boundaries shown in full lines. The plotted data also allow to draw the contour lines of u_mD/ν shown in broken lines. Regions 1 and 2 indicate the formation regions of particle waves and particle spots, respectively. The transition from Region 1 to 2 occurs when the amplitude of fluid oscillation is increased and its frequency decreased. The formation region of typical wave patterns is limited roughly to $1<u_mD/\nu<120$. Below the lower limit no particle motions occur, and above the upper limit all the particles perform the same motions.

The results of the present experiments for oscillation sand ripples are plotted in **Fig. 8** (a) with the same coordinates as those of **Fig. 7**. The plotted data allow to determine the formation regions of various ripples. The formation of rippled beds is restricted to Regions 2, 3 and 4. In Region 1, the ripples could not form even when some particles on the bed surface were in motion. In Region 5, the ripples also disappeared because of strongly oscillating beds called the

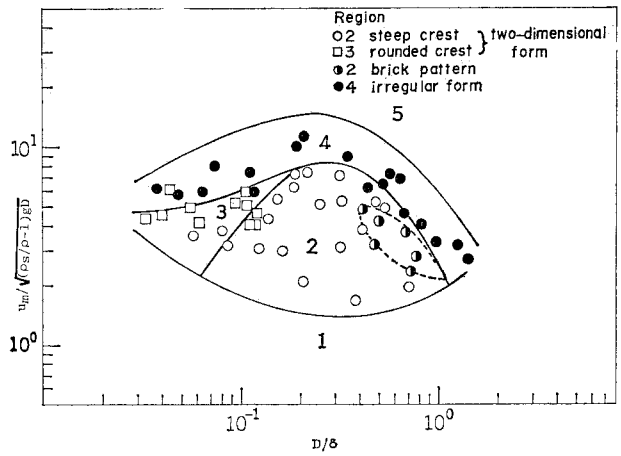

(a) Present results.

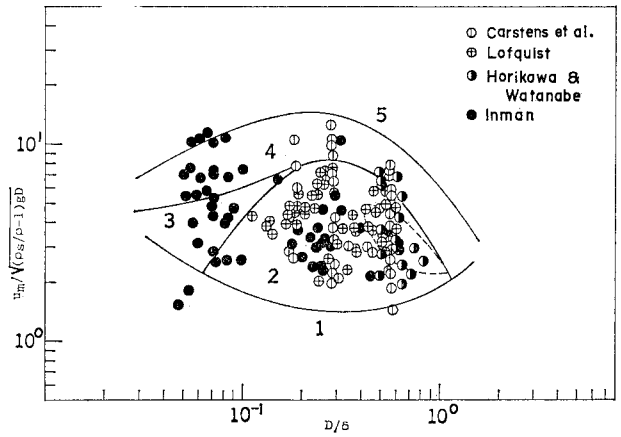

(b) Comparison with previous results.

Fig. 8 Formation Regions of Oscillation Sand Ripples.

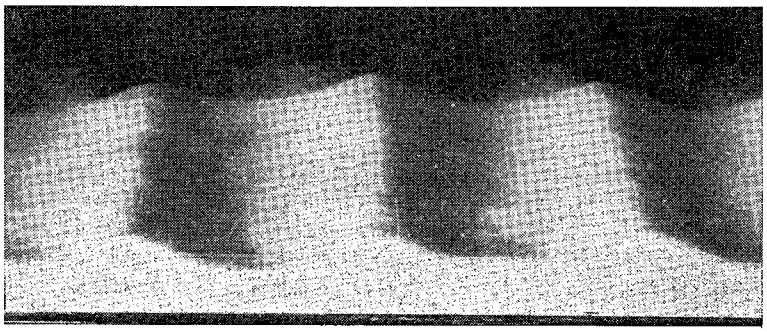

Fig. 9 Oscillation Sand Ripple with a Steep Crest.

sheet flow beds. The ripples with regular forms were observed in Regions 2 and 3. The crests were equi-spaced in the direction parallel to fluid oscillation. **Fig. 9** shows a typical form of the ripple observed in Region 2. The flow over the ripple induced vortices separated from steep ripple crests. A typical form of ripples in Region 3 are shown in **Fig. 10**. In this region, separation vortices were not induced because of large fluid viscosity, and the ripple crests were

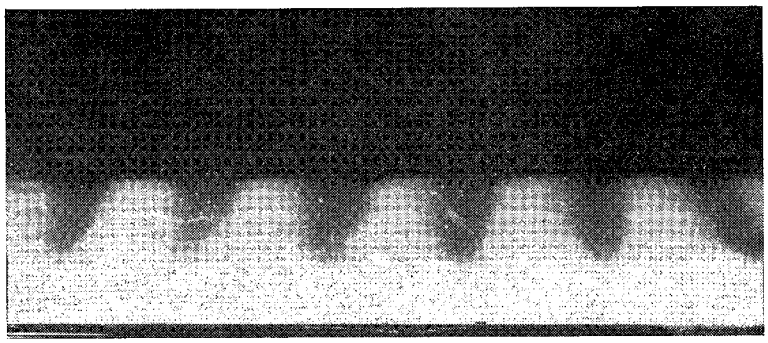

Fig. 10 Oscillation Sand Ripple with a Rounded Crest.

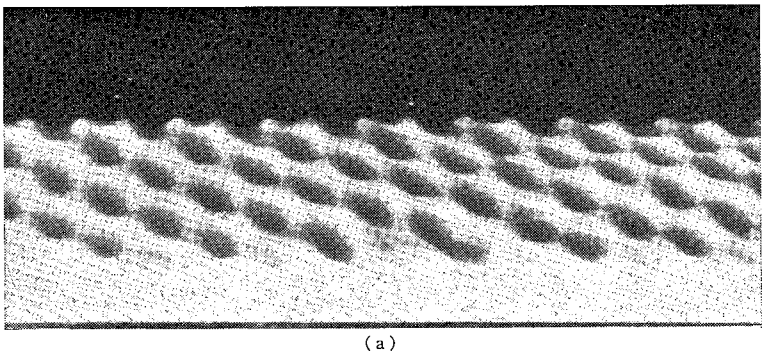

(a)

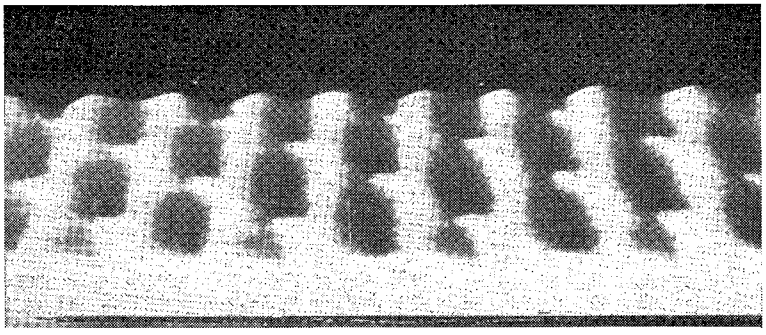

(b)

Fig. 11 Two Typical Forms of Brick Pattern Ripples.

rounded. It was reported by Kaneko & Honji[19] that in Region 3 steady streamings are observed over ripples instead of separation vortices. According to Bagnold's classification, the ripples in Regions 2 and 3 seem to correspond to vortex ripples and rolling-grain ripples, respectively. The brick pattern ripples of Bagnold[1] were observed in the region encircled by a broken line in Region 2. Two typical forms of the ripples are shown in **Figs. 11** (a) and (b). The crests were equi-spaced in two directions parallel to fluid oscillation and normal to it making up oblique patterns. Region 4 is the transition region from rippled to sheet flow beds, and the ripple forms are irregular. The critical lines for ripple initiation, transition bed and sheet flow bed agree roughly with those of Komar & Miller[10] and Dingler & Inman[11]. A similar grouping was also possible when D/δ was replaced by $u_m D/\nu$. The results of several other workers are plotted in **Fig. 8** (b) to compare with the formation regions drawn in **Fig. 8** (a). The observations of Carstens et al.[8] and Lofquist[12] in large U-tube were used as data for oscillatory flow, and the observations of Horikawa & Watanabe[7] in a wave tank and those of Inman[3] in a sea as data for water waves. The numerical data for flows and bed materials are summarized in

Table 1 Numerical Data for Flows and Bed Materials.

	Present Experiment		Carstens et al. (1969)	Lofquist (1978)	Horikawa & Watanabe (1967)	Inman (1957)
	Particle Wave	Oscillation Sand Ripple				
D (cm)	0.012—0.5	0.006—0.086	0.019—0.059	0.018—0.055	0.054	0.010—0.091
ρ_s (g/cm^3)	2.43	2.43	2.47—2.66	2.65	1.21	2.65
ρ (g/cm^3)	1.0—1.17	1.0—1.19	1.0	1.0	1.0	1.0
ν (cm^2/s)	0.0099—0.98	0.0091—2.08	0.0085—0.0107	0.01	0.0147—0.0164	0.01
d_0 (cm)	1.2—12.0	1.6—14.0	14.8—89.0	18.2—91.6	2.2—16.4	4.6—274.4
f (Hz)	0.59—2.50	0.59—2.50	0.26—0.30	0.08—0.63	0.45—1.25	0.07—1.43

Table 1. Most of the data except those of Inman fall on Region 2, and the crest of these ripples seems steep.

(3) Length-Scales of Ripples

The wavelength and the waveheight of stationary ripples are considered here. The extensive studies on the length-scales of ripples were made by Dingler & Inman[11] and Nielsen[13] by paying attention to the transition from rippled to sheet flow beds. Their results may be available for practical purposes. However, the effect of δ on ripple length-scales is overlooked in their analyses. The purpose of this section is to clarify the δ dependence of the length-scales. Attention is also focused on the particle waves in Region 1 of **Fig.** 7 and the oscillation sand ripples in Regions 2 and 3 of **Fig. 8** (a). The flow structures above these ripples agree well with those above rigid wavy walls since displacements of the particles or the rippled surfaces due to fluid oscillation are small. This agreement was mentioned previously in connection with the ripples in a highly viscous fluid. On the basis of the same dimensional analysis as that for oscillatory flow over a rigid wavy wall, the length-scales of the ripples may be described as

$$\frac{L}{d_0}=f\left(\frac{d_0}{\delta},\ \frac{H}{\delta}\right) \qquad \cdots\cdots(28)$$

in which H is equal to D for the particle waves. Symbol f stands for a function. Equation (28) is simplified more than the previous relations[4),5),11),16] based on the dimensional analyses, in which the characteristic variables of a bed material (D and ρ_s) are included. The validity of Eq. (28) is later confirmed by comparing with real ripple data. By using the steepness of ripples (H/L) Eq. (28) is rewritten as

$$\frac{H}{L}=f'\left(\frac{d_0}{\delta},\ \frac{H}{\delta}\right) \qquad \cdots\cdots(28)'$$

in which d_0/δ is equivalent to the root of the Reynolds number for oscillatory flow over a smooth plane floor and H/δ the relative roughness of ripples. Symbol f' stands for a function.

The values of L/d_0 for the data falling on Region 1 of **Fig. 7** and Regions 2 and 3 of **Fig. 8** (a) are plotted against d_0/δ in **Fig. 12** (a). The plotted data are grouped by considering the values of H/δ, and the empirical curves of Eq. (28) are drawn as the boundaries of regions. The line for Eq. (24) is also drawn in **Fig. 12** (a), and its line is in good agreement with the wavelength of real ripples for the region of $d_0/\delta<12$. It should be noted that at $d_0/\delta<12$ L depends strongly on δ and becomes much longer than d_0. Under the condition of $\epsilon\ll1$, Uda & Hino[15] and Sleath[16] suggested by means of different analytical procedures that L of ripples with a maximum growth rate depends only on δ. A comparison between their results and the present data shows that quantitative agreement is insufficient. L of particle waves becomes smaller than that of oscillation sand ripples at $d_0/\delta>12$ since particles in the waves do not pile-up. In **Fig. 12** (b), the results of present experiments for oscillation sand ripples are incorporated into those of several other workers referred previously. The previous results are extended to the region of small d_0/δ by adding the present ones. The downward scattering of Inman's data at large d_0/δ is mainly due to the data falling on Region 3 of **Fig. 8** (b). The distribution of the plotted data may allow to divide the horizontal coordinate into three regions of $d_0/\delta<12$, $12<d_0/\delta<80$, and $d_0/\delta>80$. The curves which give the best fit for $12<d_0/\delta<80$ and $d_0/\delta>80$ are respectively

$$\frac{L}{d_0}=\frac{3.08}{(d_0/\delta)^{0.353}} \qquad \cdots\cdots(29)$$

and

$$\frac{L}{d_0}=\frac{0.84}{(d_0/\delta)^{0.058}} \qquad \cdots\cdots(30)$$

It is seen from Eqs.(29) and (30) that L becomes to depend on d_0 rather than δ in the region of large d_0/δ. Flow separation over ripples may begin to occur at $d_0/\delta=12$ and develop fully at $d_0/\delta=80$. Sleath[23] computed an oscillatory viscous flow of large amplitudes over a wavy wall by means of a finite difference method and suggested a

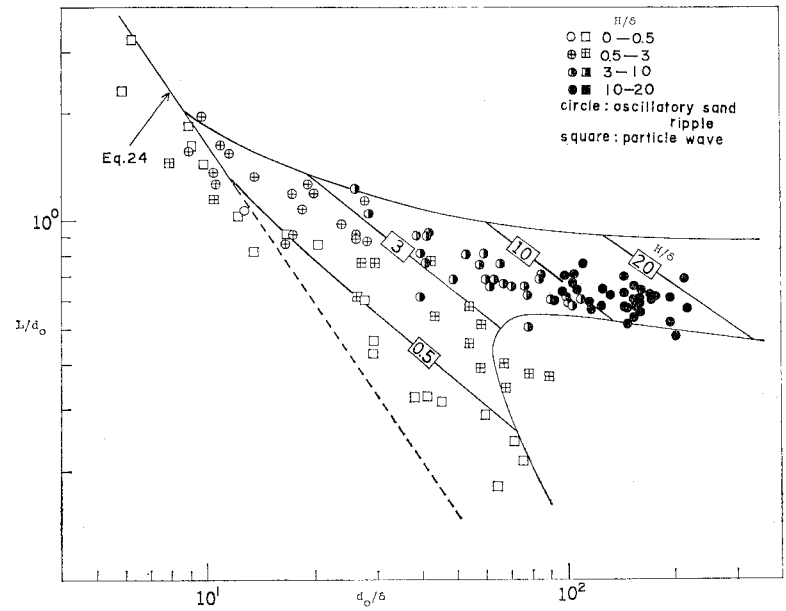

(a) Present results

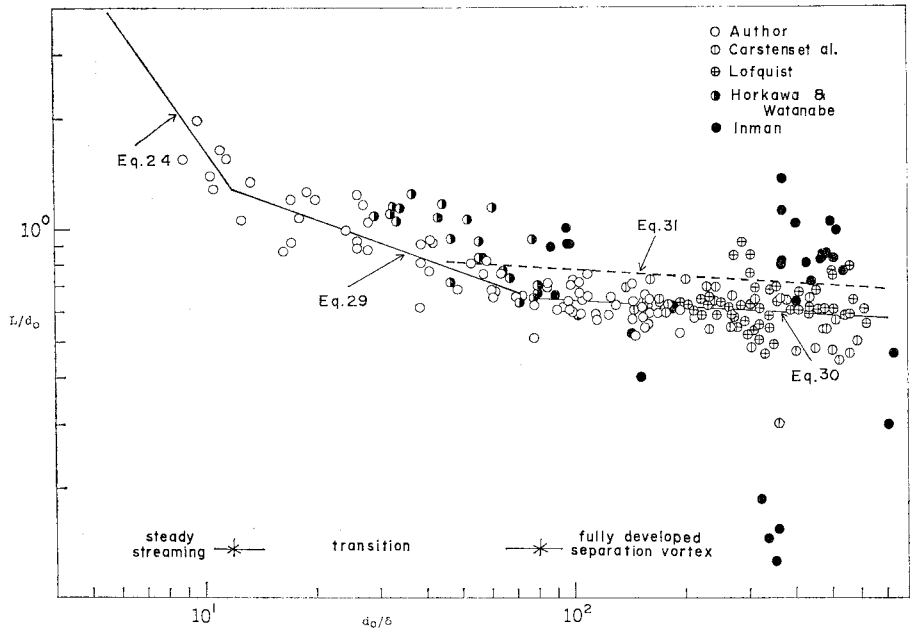

(b) Comparison with previous results

Fig. 12 Wavelength of Ripples.

relation

$$\frac{L}{d_0}=\frac{1.04}{(d_0/\delta)^{0.064}} \quad \cdots\cdots(31)$$

for the ripple wavelength with a maximum growth rate. Equation (31) agrees well with the data of real ripples at $d_0/\delta>80$ although no separation vortices appeared in the computed flow patterns.

The diagram based on Eq. (28) is shown in **Fig. 13**, in which all the ripple data including those of other workers are presented. The value of H/L in the region of $H/\delta<3$ is much smaller than that in the region of $H/\delta>10$, and the scattering of data becomes larger as d_0/δ decreases. The mean value of H/L in $H/\delta>10$ is nearly equal to that for vortex ripples by Homma &

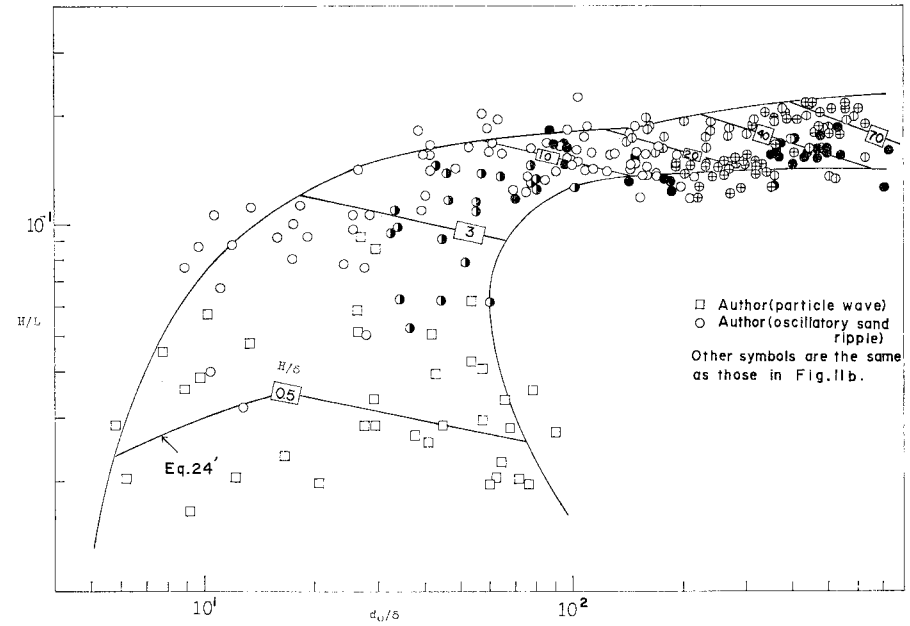

Fig. 13 Steepness of Ripples.

Horikawa[5] and Dingler & Inman[11]. The region $3<H/\delta<10$ corresponds roughly to that of $12<d_0/\delta<80$ in **Fig. 12** (b). All the data for the particle waves fall on the region of $H/\delta<3$, and the data for the brick pattern ripples scatter in the region of $5<H/\delta<15$. Equation (24) is transformed into

$$\frac{H}{L}=0.02\frac{H}{\delta}\left(\frac{d_0}{\delta}\right)^{0.48} \quad \text{for} \quad \frac{d_0}{\delta}<12 \cdots(24)'$$

The line of Eq. (24)′ for $H/\delta=0.5$ is also drawn in **Fig. 13**.

5. CONCLUSIONS

The oscillation sand ripples and the particle waves under an oscillatory flow have been observed over a wide range of fluid viscosity. The oscillatory viscous flow over a rigid wavy wall has been analysed numerically and compared with that over real ripples. Agreement between the analysis and the observation has been satisfactory. The wavelength of ripples in a highly viscous fluid has also been determined by calculating the wall shear stress due to the steady streamings. The calculated wavelength has agreed well with the experimental results at $d_0/\delta<12$. The dependence of ripple wavelength on δ has thus been clarified.

ACKNOWLEDGMENTS

The author wishes to express his thanks to Dr. H. Honji for helpful discussions and Y. Shiraishi, N. Matsunaga, and M. Kamachi for technical assistance. The computation was made by using the Melcom-Cosmo 900 of the Research Institute for Applied Mechanics, Kyushu University.

REFERENCES

1) Bagnold, R. A.: Motion of Waves in Shallow Water: Interaction between Waves and Sand Bottom, Proc. Roy. Soc. London, A-187, pp. 1–18, 1946.
2) Manohar, M.: Mechanics of Bottom Sediment Movement Due to Wave Action, U.S. Army Beach Erosion Board, TM 75, 1955.
3) Inman, D. L.: Wave-Generated Ripples in Nearshore Sands, U.S. Army Beach Erosion Board, TM 100, 1957.
4) Yalin, M. S. and R. C. H. Russel: Similarity in Sediment Transport Due to Waves, Proc. 8th Coastal Engng. Conf., Mexico City, pp. 151–167, 1962.
5) Homma, M. and K. Horikawa: Suspended Sediment Due to Wave Action, Proc. 8th Coastal Engng. Conf., Mexico City, pp. 168–193, 1962.
6) Kennedy, J. F. and N. N. Falcon: Wave-Generated Sediment Ripples, M.I.T. Hydrodynamic Lab. Rept. 86, 1965.
7) Horikawa, K. and A. Watanabe: A Study on Sand Movement Due to Wave Action, Coastal Engng. in Japan, Vol. 10, pp. 39–57, 1967.
8) Carstens, M. R., F. M. Neilsen and H. D. Altin-

bilek: Bed Forms Generated in the Laboratory under an Oscillatory Flow: Analytical and Experimental Study, U.S. Army Coastal Engng. Res. Center, TM 28, 1969.
9) Mogridge, G. R. and J. W. Kamphuis: Experiments on Bed Form Generated by Wave Action, Proc. 13th Coastal Engng. Conf. Vancouver, pp. 1123–1142, 1972.
10) Komar, P. D. and M. C. Miller: The Initiation of Oscillatory Ripple Marks and the Development of Plane-Bed at High Shear Stresses under Waves, J. Sedimentary Petrology, Vol. 45, pp. 697–703, 1975.
11) Dingler, J. R. and D. L. Inman: Wave-Formed Ripples in Nearshore Sands, Proc. 15th Coastal Engng. Conf., Hawaii, pp. 2109–2126, 1976.
12) Lofquist, K. E. B.: Sand Ripple Growth in an Oscillatory-Flow Water Tunnel, U.S. Army Coastal Engng. Res. Center, TP 78–5, 1978.
13) Nielsen, P.: Some Basic Concepts of Wave Sediment Transport, Inst. Hydrodyn. and Hydraulic Engng., Tech Univ. Denmark, Series Paper 20, 1978.
14) Chan, K. W., M. H. I. Baird, and G. F. Round: Behaviour of Beds of Dense Particles in a Horizontally Oscillating Liquid, Proc. Roy. Soc. London, A-330, pp. 537–559, 1972.
15) Uda, T. and M. Hino: A Solution of Oscillatory Viscous Flow over a Wavy Wall, Proc. Japan Soc. Civil Engineers, Vol. 237, pp. 27–36, 1975.
16) Sleath, J. F. A.: On Rolling-Grain Ripples, J. Hydraulic Res., Vol. 14, pp. 69–81, 1976.
17) Lyne, W. H.: Unsteady Viscous Flow over a Wavy Wall, J. Fluid Mech., Vol. 50, pp. 33–48, 1971.
18) Kaneko, A. and H. Honji: Initiation of Ripple Marks under Oscillating Water, Sedimentology, Vol. 26, pp. 101–113, 1979.
19) Kaneko, A. and H. Honji: Double Structures of Steady Streaming in the Oscillatory Viscous Flow over a Wavy Wall, J. Fluid Mech., Vol. 93, pp. 727–736, 1979.
20) Kaneko, A. and N. Matsunaga: Sand Ripples and Streaming in the Oscillatory Viscous Flow, Proc. 24th Japanese Conf. on Hydraulics, pp. 271–276, 1980.
21) Roache, P. J.: Computational Fluid Dynamics, Hermosa Publishers, New Mexico, 1976.
22) Honji, H., A. Kaneko and N. Matsunaga: Flows above Oscillatory Ripples, Sedimentology, Vol. 27, pp. 225–229, 1980.
23) Sleath, J. F. A.: A Contribution to the Study of Vortex Ripples, J. Hydraulic Res., Vol. 13, pp. 315–328, 1975.

(Received January 30, 1980)